
Patchiness in a minimal nutrient – phytoplankton model

HIROSHI SERIZAWA*, TAKASHI AMEMIYA and KIMINORI ITOH

Graduate School of Environment and Information Sciences, Yokohama National University, 79-7 Tokiwadai, Hodogaya-ku, Yokohama 240-8501, Japan

**Corresponding author (Fax, 81-45-339-4369; Email, seri@qb3.so-net.ne.jp)*

We present a minimal two-component model that can exhibit various types of spatial patterns including patchiness. The model, comprising nutrients and phytoplankton, includes the effect of nutrient uptake by phytoplankton as a Holling type II functional response, and also includes the effect of zooplankton grazing on phytoplankton as a Holling type II non-dynamical term. The mean-field model without the diffusion and advection terms shows both bistability and limit-cycle oscillations as a few parameters such as the input rate of nutrients and the maximum feeding rate of zooplankton are changed. If the parameter values are chosen from the limit-cycle oscillation region, the corresponding reaction–advection–diffusion equations show spatial pattern formations by the combined effects of advection and diffusion by turbulent stirring and mixing, and biological interactions. As the nutrient input is increased, the system behaviour changes from the extinction of the entire phytoplankton to the formation of filamentous patterns, patchiness patterns and homogeneous distributions. These observations suggest that the spatial pattern of phytoplankton can function as an indicator to evaluate the eutrophication level in aquatic ecosystems.

[Serizawa H, Amemiya T and Itoh K 2008 Patchiness in a minimal nutrient – phytoplankton model; *J. Biosci.* **33** 391–403]

1. Introduction

Complex systems, including ecosystems, have been known to exhibit various kinds of irregular behaviours originating from non-linearities. Some of these are occurrences of multiple stable states and catastrophic shifts between them, and the formation of various types of patterns such as patchiness and spatiotemporal chaos. In particular, pattern formation due to the effects of diffusion and/or advection has been widely investigated, constituting a fascinating field in modern natural sciences. For example, plankton patchiness has been among the central issues in mathematical modelling of aquatic ecosystems (Abraham 1998; Petrovskii and Malchow 1999; Medvinsky *et al* 2001, 2002).

Reaction–diffusion equations or reaction–advection–diffusion equations are essential tools for the investigation of pattern formation. By means of these partial differential equation systems, we can obtain various spatial patterns such as spirals, labyrinths, bands and patchiness, which are

thought to exhibit the distributions of plankton (Abraham 1998; Medvinsky *et al* 2002) or plants (von Hardenberg *et al* 2001; Rietkerk *et al* 2002).

Since the historical work of Turing (1952), numerous studies have been conducted to investigate pattern formation using reaction–diffusion equations. However, the precondition for the formation of a Turing pattern confers different diffusivities among the components; that is, the diffusivity of the activator should be less than that of the inhibitor. Once formed, the distribution of Turing patterns is stationary and spatially fixed. These restrictions complicate the application of the Turing approach to pattern formation in aquatic ecosystems, because the movement of patterns is a general phenomenon (Martin 2003).

Patchiness, as shown in figure 1, is spatial heterogeneity, which is observed in lakes, seas and oceans of various sizes. In particular, stretched and curled structures characteristic of patterns of patchiness seem to be clearly observed in seas and oceans. In fact, it is known that this kind of pattern can emerge in the mesoscale or submesoscale region from one to

Keywords. Paradox of enrichment; patchiness; reaction–advection–diffusion equations; turbulent stirring; velocity field



Figure 1. Algal blooms in the Black Sea (Credit: NASA Goddard Space Flight Center).

hundreds of kilometers, wherein lateral stirring and mixing play a more important role than vertical circulation (Martin 2003).

A number of studies have been conducted to simulate the processes of patchiness pattern formation (Abraham 1998; Medvinsky *et al* 2002). These studies seem to be classified into two groups depending on what is regarded as a major cause of these phenomena. One group focuses on biological factors such as non-linear growth and grazing interaction between phytoplankton and zooplankton (Medvinsky *et al* 2002). In contrast, another group emphasizes the effects of physical factors such as currents, eddies and the turbulent stirring induced by them (Abraham 1998).

One of the studies representative of the first group was conducted by Medvinsky *et al* (2002). They took a route different from the one taken by Turing to attain an inhomogeneous pattern formation, using a two-component model of phytoplankton and zooplankton with equal diffusivities. In spite of neglecting turbulent stirring, they succeeded in reproducing patchiness-like patterns developed from regular spirals. In their simulations, the initial spiral pattern formation is followed by its collapse, which starts near the centre, resulting in spatiotemporal

chaos in the entire region. Further, it is shown that these processes are almost independent of the initial distributions of the components. They claim that biological factors play an essential role in the emergence of plankton patchiness (Medvinsky *et al* 2002).

A number of studies have been included in the second group, where the main reason for patchiness pattern formation is considered to be physical factors (Abraham 1998; Neufeld *et al* 2002; Tzella and Haynes 2007). Most of them have adopted the three-component model comprising nutrients or their substitutes, phytoplankton and zooplankton. For example, Abraham (1998) used a model whose components are the carrying capacities and population densities of phytoplankton and zooplankton. Although the carrying capacity is frequently used as a parameter, it is, however, regarded as a variable that represents the effect of limiting nutrients in his model. The maturation time of zooplankton incorporated in this model enables fine structures to appear in the spatial distributions of the zooplankton population. In contrast, the distribution of the phytoplankton population does not show such fine structures because of their rapid growth. He adopted the seeded-eddy model (Dyke and Robertson 1985) as turbulent flows.

Another interesting issue is the pursuit of a minimal mathematical representation that can drive patchiness pattern formation. Algebraically simple models are thought to be suitable for examining the generic behaviour of the system (Scheffer 1991). Considering that continuous oscillation is required for persistent pattern formation, the minimal model should generate limit cycles in its ordinary differential equation form. It is known that two variables are sufficient for limit-cycle oscillations.

For example, Scheffer (1991) presented a minimal two-component model with phytoplankton and zooplankton, which assumed the logistic growth of phytoplankton and the Holling type II functional response in zooplankton grazing on phytoplankton. Without considering fish predation, the local kinetics of the model show a typical phytoplankton–zooplankton limit-cycle oscillation. Moreover, the addition of a non-dynamical fish predation term with the Holling type III functional response gives the possibility of bistable behaviours.

Petrovskii and Malchow (1999) first attempted to apply the Sheffer model to pattern formation in one-dimensional reaction–diffusion equations. This was the first study to show chaotic pattern formation in a reaction–diffusion system with equal diffusivities, where they emphasized the importance of including the unstable fixed point in initial distributions. Thereafter, the application has been extended to two-dimensional models in the following studies such as the one by Medvinsky *et al* (2002).

Rietkerk *et al* (2004) suggested a predictable sequence of emerging self-organized patchiness as the resource input decreases or increases, referring to the vegetation patterns in arid ecosystems. A sequence of vegetation patterns induced by decreased rainfall emerges in the next order, namely, homogeneous cover, gaps, labyrinths or stripes, and spots. We expect to find a similar succession of spatial patterns in aquatic ecosystems.

Consequently, the objectives of the present study can be summarized as follows: (i) to propose an alternative minimal two-component model with nutrients and phytoplankton, which can create persistent spatial patterns, and (ii) to determine a sequence of algal distribution patterns in aquatic ecosystems as the environmental factors change.

Initially, we aimed to construct the algebraically simple mean-field model that can produce limit-cycle oscillations. Subsequently, we modified it to reaction–advection–diffusion equations by adding diffusion terms with equal diffusivities and advection terms induced by simple turbulent stirring. Within a certain range of nutrient input level, our model shows various types of pattern formation. However, a further increase in nutrient loading, which means the progress of eutrophication, makes the system converge to a stable equilibrium state. The return to homogeneous distribution means that adoption of the two-component model with

nutrients and phytoplankton is one of the possible ways to avoid continuing limit-cycle oscillations of increasing amplitude, which could increase the stochastic possibility of species extinction (Rosenzweig 1971).

2. Methods

2.1 Mean-field model

We begin with the so-called mean-field model, which is represented by ordinary differential equations. Our two-component model is described as follows:

$$\frac{dN}{dT} = I_N - k\mu \frac{N}{H_N + N} P - m_N N, \quad (1)$$

$$\frac{dP}{dT} = \mu \frac{N}{H_N + N} P - f_p \frac{P}{H_p + P}. \quad (2)$$

Here, two variables N and P denote the nutrient concentration and phytoplankton density, which are functions of the actual time T . We assume that the nutrient is phosphorus. With regard to the parameters, I_N is the input rate of nutrients from the environment, μ is the maximum growth rate of phytoplankton, k is the nutrient content in phytoplankton, m_N is the removal rate of nutrients, f_p is the maximum predation rate of zooplankton on phytoplankton, and H_N and H_p are the half-saturation constants of nutrients and phytoplankton, respectively. The uptake of nutrients by phytoplankton is represented by the Holling type II functional response. Moreover, the implicitly assumed zooplankton grazing on phytoplankton is incorporated as a non-dynamical term, which is also formulated by the Holling type II functional response. The parameter values assumed in this study are listed in table 1.

The use of the Holling type II functional response in zooplankton grazing on phytoplankton is crucial to our model, in spite of the fact that it is formulated as a non-dynamical term. This type of functional response has been broadly adopted to describe zooplankton predation in many theoretical studies (Holling 1973; Scheffer 1991; Petrovskii and Malchow 1999; Medvinsky *et al* 2002). It is also reported that the Holling type II functional response shows good concordance with experimental data (Mullin *et al* 1975; Gentleman *et al* 2003).

The removal term of nutrients $m_N N$ is added to evaluate the losses except for the uptake by phytoplankton, such as sedimentation to a deep bottom or an outflow from the system. However, this term has another meaning in terms of mathematical modelling. Suppose that phytoplankton is completely extinct. In this extreme case, the nutrient concentration N continues to increase unlimitedly. We intend to avoid this unfavourable situation by adding the removal term. We can also confirm that the simulation results for

Table 1. Parameter values in mathematical model (1)–(2)

Parameters	Meaning	Values	Units	References
I_N	Input rate of nutrient	0.00225	$\text{g}\cdot\text{m}^{-2}\cdot\text{day}^{-1}$	0.00005–0.002 ^(b) , 0.0–0.0015 ^(c)
μ	Maximum growth rate of phytoplankton	0.5	day^{-1}	0.2–8.0 ^(a) , 0.3 ^(b)
k	Nutrient content in phytoplankton	0.01		0.0088–0.033 ^(a) , 0.02 ^(b)
m_N	Loss rate of nutrient	0.015	day^{-1}	0.005 ^(b)
f_p	Maximum feeding rate of zooplankton on phytoplankton	1.8, 2.0	$\text{g}\cdot\text{m}^{-2}\cdot\text{day}^{-1}$	0.045–13.8 ^(a) , 2.0 ^(b)
H_N	Half-saturation constant of nutrient	0.005	g/m^2	0.0005–0.08 ^(a) , 0.005 ^(b)
H_p	Half-saturation constant of phytoplankton	4.0	g/m^2	$\sqrt{60.0}$ ^(b) , $\sqrt{6.0}$ ^(c)

The parameter values assumed in this study were determined by referring to the following studies: (a) Bowie *et al* (1985), (b) DeAngelis *et al* (1989), and (c) Amemiya *et al* (2005). By the use of these parameter values, we intend to describe aquatic ecosystems in which algal blooms can occur. The referenced value of k from (a) is for the phosphorus composition of algal cells. The referenced values of H_p are converted to their square roots because of the use of a Holling type III functional response in the studies (b) and (c).

spatial pattern formation are fundamentally not altered, even if this term is omitted.

Different from the two-component model by Scheffer (1991), our model consists of nutrients and phytoplankton. This is the most striking difference between the Scheffer model and ours. In the Scheffer model, the nutrient concentration of the system is estimated by the carrying capacity as a parameter, whereas it is an explicit state variable in our model. Meanwhile, the effect of zooplankton grazing on phytoplankton is included as a non-dynamical term in our model, whereas its density is an explicit state variable in the Scheffer model. In summary, our model emphasizes the uptake of nutrients by phytoplankton, while the Scheffer model attaches importance to the grazing activity of zooplankton on phytoplankton.

One of the motivations for initiating this study is to offer an alternative minimal two-component model to Scheffer’s one. In this sense, our current study is based on theoretical interest. It is certain that the adoption of a non-dynamical term for zooplankton predation means a constant zooplankton density. However, our major concern is not about the temporal change in total biomass over a long term but about the change in spatial distributions over a comparatively short term. Our assumption that the zooplankton density is constant could be justified for a short period. Therefore, the two-component model with nutrients and phytoplankton could have the reality to describe some aspects of the spatiotemporal dynamics of algae.

2.2 Dimensionless representation

Dimensionless variables are introduced in order to reduce the number of parameters:

$$t = \mu T, n = \frac{N}{H_N}, p = \frac{P}{H_p}. \tag{3}$$

Table 2. Parameter values in mathematical models (5)–(6) and (7)–(9)

Parameters	Conversion or meaning	Set I	Set II
i_n	$=I_N\mu^{-1}H_N^{-1}$	0.9	1.8
a	$=kH_pH_N^{-1}$	8.0	8.0
m_n	$=m_N\mu^{-1}$	0.03	0.03
f_p	$=f_p\mu^{-1}H_p^{-1}$	0.9	1.0
d	Diffusion coefficient	0.04	
v_{\max}	Maximum velocity	0.3	
L	Half length of square domain side	100	
A	Scale factor for initial distributions of n and p	0.25, 0.5, 1.0	

The parameter values used in the mathematical models (5)–(6) and (7)–(9) were derived from those in table 1. The values of i_n and A are changed as control parameters. The simulations of pattern formation by the mathematical model (7)–(9) were performed only for the parameter set I.

Then, we use the following dimensionless parameters:

$$i_n = \frac{I_N}{\mu H_N}, a = \frac{kH_p}{H_N}, m_n = \frac{m_N}{\mu}, f_p = \frac{f_p}{\mu H_p} \tag{4}$$

As a result, we obtain the subsequent simplified representation:

$$\frac{dn}{dt} = i_n - a \frac{n}{1+n} p - m_n n, \tag{5}$$

$$\frac{dp}{dt} = \frac{n}{1+n} p - f_p \frac{p}{1+p}. \tag{6}$$

Newly adopted dimensionless variables n , p and t represent ratios relating to the relative amounts of nutrient concentration, phytoplankton density and time, respectively.

The values of dimensionless parameters listed in table 2 are derived from those in table 1.

2.3 Velocity field

Turbulent stirring is considered to be a crucial factor in creating patchiness patterns in aquatic ecosystems. In this study, we use a two-dimensional turbulent flow developed by referring to the seeded-eddy model (Dyke and Robertson 1985; Abraham 1998). The stream function ψ and the fluid velocity \mathbf{v} are described as follows:

$$\psi(x, y) = s \sum_i \sigma_i \exp \left\{ -\frac{(x - x_i)^2 + (y - y_i)^2}{r_0^2} \right\}, \quad (7)$$

$$\sigma_i = 1 \text{ or } -1, \quad \mathbf{v} = (v_x, v_y) = \left(-\frac{\partial \psi}{\partial y}, \frac{\partial \psi}{\partial x} \right).$$

The velocity field created by turbulent stirring is constructed by the superimposition of 100 eddies, half of which rotate clockwise, while the other half rotate counterclockwise. In our model, the centre of each eddy (x_i, y_i) is randomly distributed within the domain. For simplicity, we use a constant value of radius r_0 for all eddies without considering a distribution of varying eddy sizes. However, it is confirmed that no essential difference is observed in the final appearance of patchiness patterns as compared with a case in which the radius is varied. The scaling constant s is introduced in order to adjust the maximum velocity v_{\max} .

The domain in our simulations is a 200×200 square, that is, a half length of each side is $L=100$. The radius of each eddy is $r_0=10$, and the maximum velocity is $v_{\max}=0.3$. The velocity field is stationary and remains temporally unchanged.

2.4 Reaction–advection–diffusion equations

The reaction–advection–diffusion equations for the present model are described as follows:

$$\frac{\partial n}{\partial t} = d \nabla^2 n - \nabla \cdot (\mathbf{v}n) + i_n - a \frac{n}{1+n} p - m_n n, \quad (8)$$

$$\frac{\partial p}{\partial t} = d \nabla^2 p - \nabla \cdot (\mathbf{v}p) + \frac{n}{1+n} p - f_p \frac{p}{1+p}. \quad (9)$$

$$\nabla = \left(\frac{\partial}{\partial x}, \frac{\partial}{\partial y} \right), \quad \nabla^2 = \frac{\partial^2}{\partial x^2} + \frac{\partial^2}{\partial y^2}.$$

The last two formulae specify the Laplacian operators. Two dimensionless variables x and y denote the position coordinates. The dimensionless parameter d is the diffusion coefficient, whose value is also shown in table 2. We assume that the lateral diffusivities are equal for both components,

which is the usual case for passive tracers such as nutrients and phytoplankton.

In our spatiotemporal simulations, the two-dimensional square domain is divided into a rectangular grid of 180×180 cells. Therefore, each cell is a 1.11×1.11 square, and the velocity vector is allocated to each cell. The fourth-order Runge–Kutta integrating method is applied with a time step $\Delta t=0.12$ to 0.36 , depending on the program. It is confirmed that the results with smaller time steps remain the same for each program, ensuring the accuracy of the simulations. The use of a larger time step is only for the purpose of speedy calculations.

2.5 Initial and boundary conditions

In our simulations of the partial differential equation system (7)–(9), the initial distributions of n and p are given by the following equations, respectively:

$$n(x, y, 0) = n_1 \left(1 + A \sin \frac{\pi}{L} x \right), \quad (10)$$

$$p(x, y, 0) = p_1 \left(1 + A \sin \frac{\pi}{L} y \right). \quad (11)$$

Here, n_1 and p_1 denote the values of two components at the unstable fixed point F_1 , which is explained later. Another parameter A is the scale factor for initial distributions of n and p . The distributions of both n and p , as well as their first-order derivatives, are continuous throughout the boundaries. In addition, the gradients of the two components are perpendicular to each other. These initial conditions are used together with the periodic boundary conditions.

In fact, the process of patchiness pattern formation is almost independent of the initial conditions. However, it is at least required to include the values at the unstable fixed point F_1 , which functions as a seed for irregular pattern formation (Petrovskii and Malchow 1999).

3. Results

3.1 Fixed points

Prior to the examination of pattern formation by the partial differential equation system (7)–(9), it is useful to investigate the corresponding ordinary differential equation system (5)–(6). In order to calculate the position of fixed points, we solved the following simultaneous equation:

$$i_n - a \frac{n}{1+n} p - m_n n = 0, \quad (12)$$

$$\frac{n}{1+n} p - f_p \frac{p}{1+p} = 0. \quad (13)$$

This simultaneous equation (12)–(13) gives three fixed points, one of which is easily identified as follows:

$$F_0 \left(\frac{i_n}{m_n}, 0 \right). \tag{14}$$

Another two fixed points can be obtained by solving the following quadratic equation for n :

$$n^2 + \frac{af_p - i_n - a + m_n}{m_n} n + \frac{af_p - i_n}{m_n} = 0, \tag{15}$$

$$p = \frac{f_p}{n} + f_p - 1.$$

Denoting two solutions of the quadratic equation as n_1 and n_2 , we can obtain the other two fixed points, as follows:

$$F_1 \left(n_1, \frac{f_p}{n_1} + f_p - 1 \right), F_2 \left(n_2, \frac{f_p}{n_2} + f_p - 1 \right). \tag{16}$$

Here, we denote the three fixed points as F_0 , F_1 and F_2 .

3.2 Stability analyses

The stability of the system (5)–(6) can be analysed at each fixed point using the following characteristic equation:

$$\begin{vmatrix} -\frac{ap}{(1+n)^2} - m_n - \lambda & -\frac{an}{1+n} \\ \frac{p}{(1+n)^2} & \frac{n}{1+n} - \frac{f_p}{(1+p)^2} - \lambda \end{vmatrix} = 0. \tag{17}$$

This is a quadratic equation for λ , which denotes the eigenvalue in each fixed point. If the real parts of eigenvalues are all negative, the corresponding fixed point is stable. Otherwise, the fixed point is unstable.

We conducted stability analyses for two sets of parameters, i.e. set I and set II in table 2, the results of which are shown in tables 3 and 4, respectively. For the parameter set I, the system has two fixed points under the conditions that both components n and p are 0 or positive ($n \geq 0$ and $p \geq 0$). These are the unstable saddle point F_0 and node F_1 . Considering that $p = 0$ at F_0 , this fixed point is referred to as a nutrient-dominated (ND) state, while F_1 is, in contrast, referred to as a phytoplankton-dominated (PD) state.

Meanwhile, for the parameter set II, three fixed points are generated, which are identified as one stable attractor F_0 and two unstable fixed points F_1 and F_2 . The attractor F_0 is identified as the ND state, while F_1 corresponds to the PD state. The bifurcation diagrams will be shown later for both of the parameter sets I and II.

3.3 Dependence of system behaviour on parameters

Figure 2 shows the parameter regions related to different behaviours in terms of the input rate of nutrients i_n and the maximum feeding rate of zooplankton f_p . The system behaviours are classified into six categories: (i) the convergence to a stable ND state F_0 (the white region in the upper left area), (ii) the convergence to a stable PD state F_1 (the black region), (iii) the limit-cycle oscillation around the unstable fixed point F_1 (the white region at the centre), (iv) bistability between (i) and (ii) (the dark-grey region), (v) bistability between (i) and (iii) (the light-grey region), and (vi) divergence (not shown). Two black symbols "x" in the areas (iii) and (v) represent the values of the parameter sets I and II in table 2, respectively.

Two typical limit-cycle oscillations are shown in figure 3, corresponding to the parameter sets I and II. The positions of the fixed points within the realistic range ($n \geq 0$ and $p \geq 0$) are also shown in figure 3. There are two fixed points,

Table 3. Stability analyses for parameter set I in mathematical model (5)–(6)

	(n, p)	Eigenvalues	Stability	Fixed points	States
F_0	(30.0, 0.0)	0.068, -0.03	Unstable	Saddle point	ND
F_1	(4.07, 0.121)	0.01±0.156i	Unstable	Unstable node	PD

The mathematical model (5)–(6), consisting of the nutrient concentration n and the phytoplankton density p , generates two unstable fixed points within the region $n \geq 0$ and $p \geq 0$ for the parameter set I in table 2. These are the saddle point F_0 and unstable node F_1 . Considering that $p=0$ at F_0 , this fixed point is referred to as a nutrient-dominated (ND) state, while F_1 is referred to as a phytoplankton-dominated (PD) state.

Table 4. Stability analyses for parameter set II in mathematical model (5)–(6)

	(n, p)	Eigenvalues	Stability	Fixed points	States
F_0	(60.0, 0.0)	-0.016, -0.03	Stable	Attractor	ND
F_1	(3.74, 0.267)	0.021±0.232i	Unstable	Unstable node	PD
F_2	(55.26, 0.018)	0.016, -0.029	Unstable	Saddle point	

The mathematical model (5)–(6) with the parameters for the parameter set II generates one attractor F_0 and two unstable fixed points F_1 and F_2 .

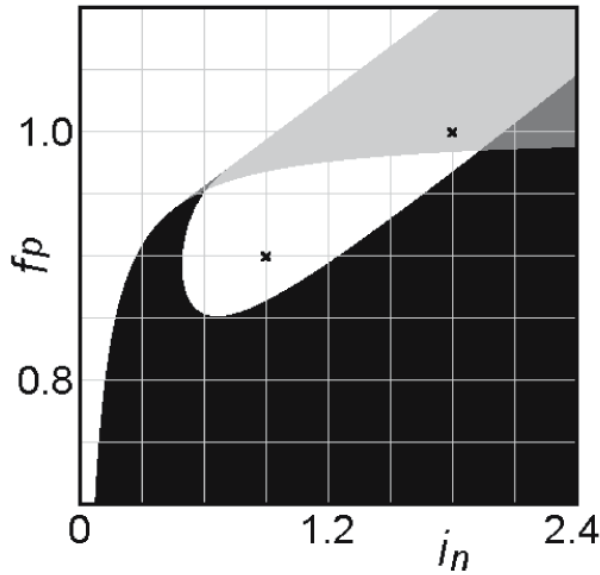


Figure 2. Parameter regions corresponding to different behaviours. The system shows six different behaviours, depending on the parameter values. These are (i) the convergence to the stable nutrient-dominated (ND) state (the white region in the upper left), (ii) the convergence to the stable phytoplankton-dominated (PD) state (the black region), (iii) the limit-cycle oscillation around the unstable fixed point (the white region at the centre), (iv) bistability between (i) and (ii) (the dark-grey region), (v) bistability between (i) and (iii) (the light-grey region) and (vi) divergence (not shown). Two black symbols "x" show the values of the parameter sets I and II in table 2.

F_0 (unstable) and F_1 (unstable), in (a), and three fixed points, F_0 (stable), F_1 (unstable), and F_2 (unstable), in (b).

3.4 Bifurcation diagrams

Figure 4 (a) and (b) show the bifurcation diagrams of the nutrient concentration n (a) and the phytoplankton density p (b) for the parameter set I as a function of the input rate of nutrients i_n . Each bifurcation diagram consists of two branches. The first straight branch is referred to as an ND branch in which phytoplankton cannot survive, while n increases linearly with i_n . In the case that the maximum zooplankton feeding rate $f_p < 1$, there exists a transcritical point i_{tc} , which is described by

$$i_{tc} = \frac{m_n f_p}{1 - f_p}. \tag{18}$$

In the region $i_n \leq i_{tc}$, the equilibrium state in the ND branch is stable, while the state is unstable in $i_n > i_{tc}$. In the case of the parameter set I, the transcritical point $i_{tc} = 0.27$.

Meanwhile, the other curved branch is referred to as a PD branch, where nutrients and phytoplankton coexist ($n > 0$ and $p > 0$). The PD branch is connected to the ND branch at the transcritical point i_{tc} . There exist two Hopf bifurcation points $i_{n0} = 0.495$ and $i_{n1} = 1.247$ in the PD branch, between which the system exhibits limit-cycle oscillations. Consequently, the system shows limit-cycle oscillations within the intermediate region $i_{n0} < i_n < i_{n1}$, while it converges to a stable equilibrium state in the region $0 < i_n \leq i_{n0}$ or $i_n \geq i_{n1}$.

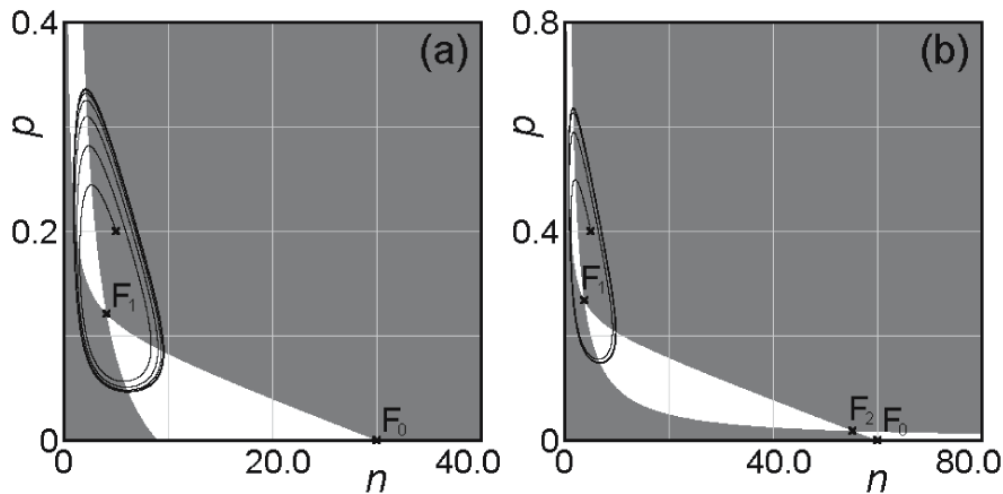


Figure 3. Limit cycles in mathematical model (5)–(6). (a) shows the trajectory of the limit-cycle oscillation by the parameter set I in table 2, while (b) shows that by the parameter set II. The state variables move on the phase plane to the upper-right direction or the lower-left direction in the white regions and the upper-left direction or the lower-right direction in the grey regions. Two unstable fixed points exist in (a), which are F_0 in the ND branch and F_1 in the PD branch. Meanwhile, one stable attractor F_0 and two unstable fixed points F_1 and F_2 are shown in (b).

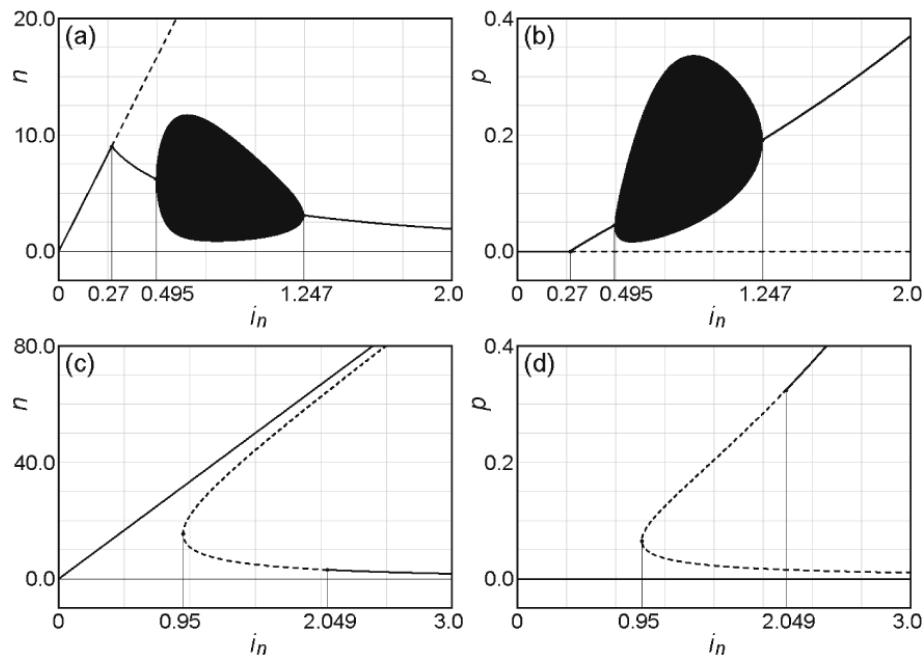


Figure 4. Bifurcation diagrams in mathematical model (5)–(6). These are the bifurcation diagrams of the nutrient concentration n and the phytoplankton density p as a function of the nutrient input rate i_n . (a) and (b) are the case of limit-cycle oscillations by the parameter set I in table 2, while (c) and (d) are the case of bistability by the parameter set II. The solid lines represent the stable attractors, while the broken lines represent the unstable saddle points or nodes. The black areas represent limit-cycle oscillations.

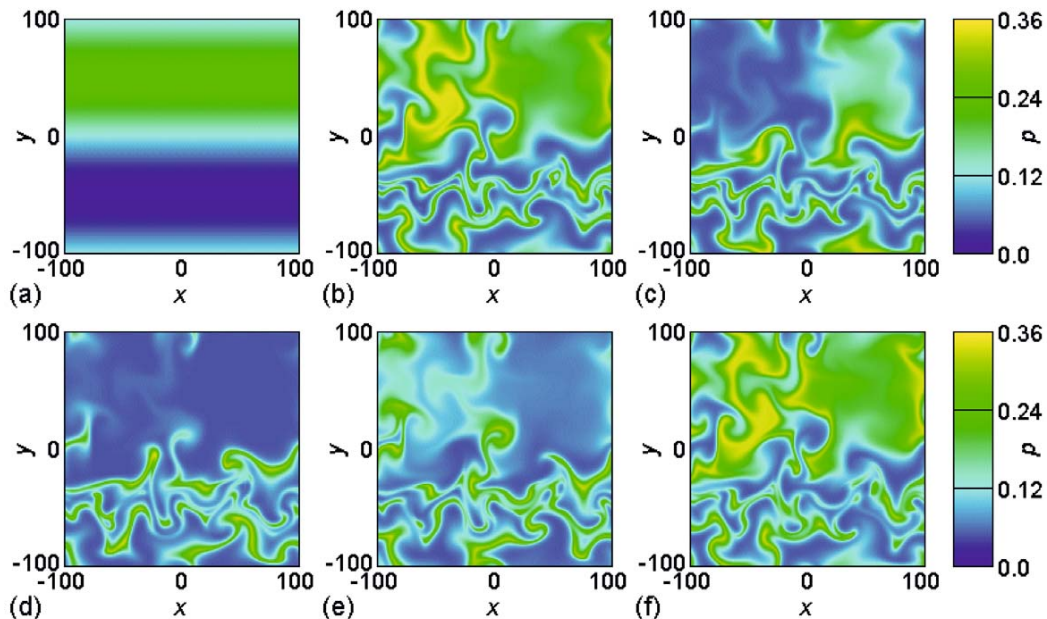


Figure 5. Temporal change in spatial distribution of phytoplankton in mathematical model (7)–(9). The initial distributions of the nutrient concentration n and the phytoplankton density p are given by the equations (10)–(11). Periodic boundary conditions are imposed. The obvious similarity between the two images in (b) and (f) indicates that the temporal variation of the system shows periodicity in a time cycle of about 45 units, which is also the period of the limit-cycle oscillation. $A=1.0$. (a) $t=0$, (b) $t=135$, (c) $t=144$, (d) $t=156$, (e) $t=168$, (f) $t=180$.

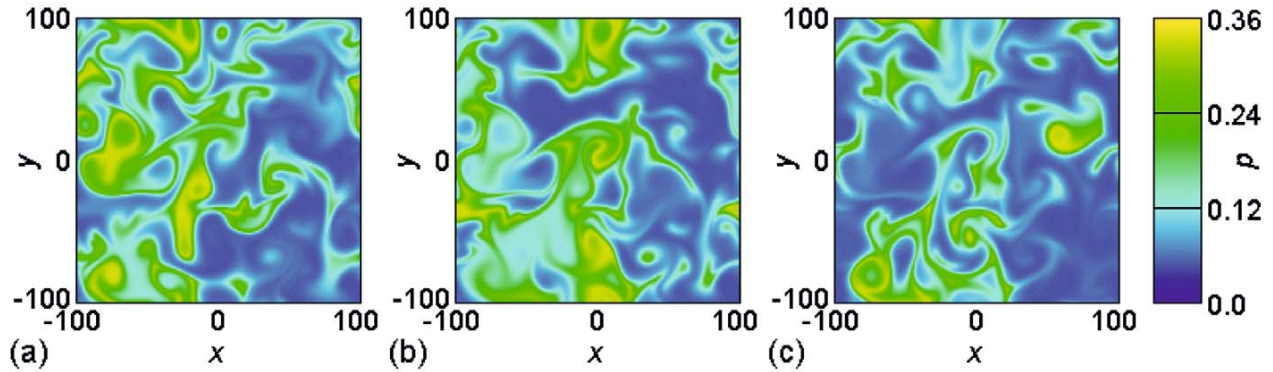


Figure 6. Dependence of spatial distribution of phytoplankton density on initial conditions after a long period of time in mathematical model (7)–(9). The initial distributions are given by the equations (10)–(11), and periodic boundary conditions are imposed. $t=1800$. (a) $A=0.25$, (b) $A=0.5$, (c) $A=1.0$.

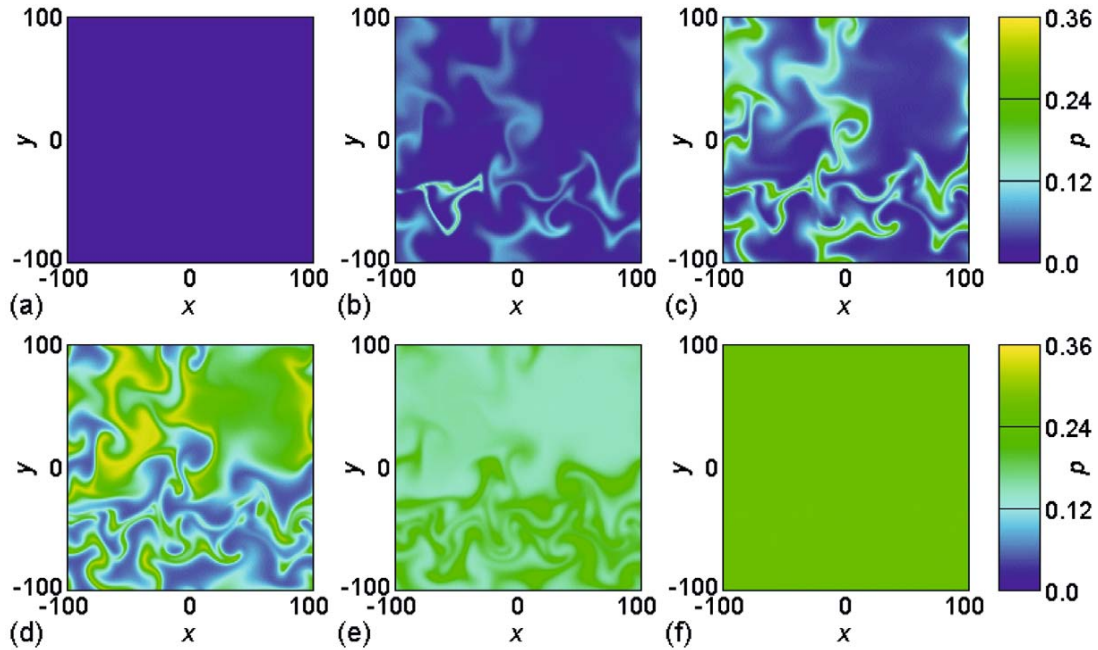


Figure 7. Dependence of spatial distribution of phytoplankton density on nutrient input rate in mathematical model (7)–(9). The initial distributions are given by the equations (10)–(11), and periodic boundary conditions are imposed. $t=180$, $A=1.0$. (a) $i_n=0.2$, (b) $i_n=0.5$, (c) $i_n=0.7$, (d) $i_n=0.9$ (same as figure 5f), (e) $i_n=1.25$, (f) $i_n=1.6$.

Figure 4c and d are the bifurcation diagrams of n (c) and p (d) for the parameter set II as a function of i_n . Although both the straight ND branch and the curved PD branch can be observed, these are not connected with each other. It is obvious from the equation (18) that the transcritical point cannot exist in the case of $f_p \geq 1$ within the realistic region $i_n \geq 0$. In this case, equilibrium states are always stable in the ND branch for all i_n . The system shows bistability between the convergence to two stable attractors F_0 and F_1 in a region $i_n \geq 2.049$. Meanwhile, bistability could occur between the

convergence to a stable attractor F_0 and the limit-cycle oscillation around an unstable fixed node F_1 within a region $0.95 \leq i_n < 2.049$.

3.5 Spatial pattern formation

The spatiotemporal behaviours of the reaction–advection–diffusion equations (7)–(9) are shown in figures 5, 6 and 7 for the parameter set I in table 2. Figure 5 shows the temporal change of the spatial distribution of phytoplankton.

The similarity seen between the two images (b) and (f) is obvious, indicating that the spatial pattern varies periodically in an approximately 45-unit time cycle corresponding to the period of the limit-cycle oscillation.

The dependence of spatial phytoplankton distribution on the initial condition is examined at $t=1800$ for three cases, $A=0.25, 0.5$ and 1.0 , in figure 6. After a long period of time, the spatial distributions become quite different from each other, reflecting the sensitivity to the initial conditions, which is a characteristic feature of chaotic systems. However, it is clear that the spatial distributions continue to change without decaying to homogeneous ones.

Meanwhile, in figure 7, the dependence of the spatial distributions of p on i_n is investigated at $t=180$. Various types of spatial patterns can be observed in the region $i_n > 0.495$ including a homogeneous distribution. In particular, mildly stretched and curled structures, as shown in figure 7d, seem to replicate real plankton patchiness as seen in figure 1.

4. Discussion

4.1 Diffusion and advection

There are two types of diffusion. The first type of diffusion is usual diffusion in the context of molecular hydrodynamics, which is thought to be a tendency toward homogeneity originating from the second law of thermodynamics. Therefore, it is effective without any physical water flow. This type of diffusion is represented by the first terms on the right side in equations (8) and (9), which are referred to as diffusion terms in this article. On the other hand, the second type of diffusion is diffusion by advection. Advection is substantial water flow such as currents and eddies, and diffusion by advection is passive movement carried by advection. Therefore, it is ineffective within perfectly calm water. This type of diffusion is represented by the second terms on the right side in equations (8) and (9), referred to as advection terms. The actual mixing of nutrients or phytoplankton is caused by a combination of these two effects. However, the main cause of pattern formation in the water area assumed in this study is not the first type of diffusion but the second type, that is, diffusion by advection.

From the technical point of view, diffusion terms are required for smoothing the pattern. Without diffusion terms, the difference in values between adjacent cells often soars, which could lead the simulation system to divergence. In order to avoid it, the time step and/or the cell size should be very small, resulting in a long simulation time. Therefore, the parameter d does not mean a real diffusion coefficient but a kind of smoothing factor in the current computer simulations.

In our model, the real diffusion coefficient D can be evaluated by the following equation:

$$D = \mu L_D^2. \quad (19)$$

As a rough approximation, suppose that the domain is 200×200 km², the maximum growth rate of phytoplankton μ is 0.5 day⁻¹, and that the characteristic scale of diffusion L_D is given by the maximum velocity v_{\max} . In this case, $L_D = 0.3$ km, then, we can estimate the value of turbulent diffusivity D as 0.045 km²/day. This value is converted to about 5×10^3 cm²/s, which is in agreement with the empirical data estimated by Okubo (1971) that range from 5×10^2 to 2×10^6 cm²/s.

4.2 Paradox of enrichment

The input of nutrients is one of the most critical external factors that can promote eutrophication in aquatic ecosystems. Therefore, understanding the correlation between the nutrient loading level and spatial patterns of phytoplankton blooms is important for predicting the degradation of aquatic ecosystems. Even in the mean-field model, where the heterogeneity of spatial distributions is neglected, the transition in algal blooming states is expected.

Figure 4b shows a bifurcation diagram of p , which emphasizes the limit-cycle oscillations in a range of $0.495 < i_n < 1.247$. This diagram is regarded as a section of figure 2 at $f_p = 0.9$. Figure 4b clearly shows the transition of the phytoplankton density p from extinction to homogeneous cover with a small amount of phytoplankton, limit-cycle oscillations and mass occurrence without oscillation, as the nutrient input is increased. Within the limit-cycle oscillation region, the amplitude varies as eutrophication progresses, showing a peak near $i_n = 0.9$. Meanwhile, within the mass occurrence region ($i_n \geq 1.247$), the value of p increases rapidly with an increase in the nutrient input.

The paradox of enrichment has been a controversy among theoretical ecologists (Roy and Chattopadhyay 2007). According to it, an increase in the nutrient input can destabilize a prey–predator system and even lead to the extinction of species (Rosenzweig 1971; Petrovskii *et al* 2004). In some mathematical models, it has been theoretically shown that an increase in the carrying capacity of the environment, which is considered to be caused by enrichment or eutrophication, leads to population oscillations of increasing amplitude (Scheffer 1998). As a result, the minimum value of the population density decreases and species extinction becomes more probable due to stochastic environmental perturbations (Petrovskii *et al* 2004). Although the extinction of a prey–predator community following system eutrophication has been observed in some laboratory experiments (Luckinbill 1974; Bohannan and Lenski 1997), this kind of phenomenon

is not commonly seen in nature (McCauley and Murdoch 1990; Petrovskii *et al* 2004).

For example, the paradox of enrichment can be seen in a two-component model adopted by Scheffer (1991) and Medvinsky *et al* (2002). In this model, which consists of phytoplankton and zooplankton, it is shown that an increase in the carrying capacity causes a continuous increase in the amplitude of limit-cycle oscillations. In order to avoid the paradox of enrichment, some kinds of mechanisms have been proposed. For example, it is claimed that the paradox can be resolved by the transition to spatiotemporal chaos (Petrovskii *et al* 2004) or by inducible defences (Vos *et al* 2004). Scheffer (1998) also claimed that the presence of inedible algae such as large cyanobacterial colonies and spatial heterogeneity are potential stabilizing mechanisms.

It should be noted that our two-component model (5)–(6) does not exhibit the paradox of enrichment. As shown in figure 4b, the limit-cycle oscillations in our model are restricted in a certain range of the nutrient input ($0.495 < i_n < 1.247$), and a further increase in the nutrient input makes the system return to convergence to a stable equilibrium state. Considering that an increase in the nutrient input is equivalent to an increase in the carrying capacity, our nutrient–phytoplankton model is likely to be one of the counter-examples of the paradox for ecological modelling.

4.3 Temporal change in spatial pattern of phytoplankton density

Figure 5 shows the temporal change in spatial distribution of phytoplankton. As shown in figure 5b, the typical patchiness pattern formation with stretched and curled structures is completed within 135 unit times. These features of patchiness patterns are supposed to be due to the coupled effects of stretching by currents and turbulent stirring by eddies. It should be noted that the appearance of the pattern is not induced by the initial conditions. The initial conditions are chosen so that the spatial distributions do not show any spatial symmetry. The initial distributions represented by (10)–(11) seem to be one of the simplest forms that satisfies this condition and is also consistent with the periodic boundary conditions.

One of the characteristic features seen in the temporal change of phytoplankton distribution is its periodic behaviour. As shown in the two images in figure 5b and f, and similar patterns appear periodically without decaying to homogeneous distributions. The period is estimated at about 45 unit times, which is also thought to be equal to the period of the limit-cycle oscillation.

As shown in figure 6, the spatial variability of phytoplankton distribution is not damped out with time, regardless of the initial conditions. As the parameter i_n

is spatially uniform, the spatial distributions are homogeneous unless the initial conditions are heterogeneous. However, the heterogeneous flow of turbulent stirring that operates as an external force generates persistently changing spatial patterns in our model, coupled with heterogeneity in the initial distributions of nutrients and phytoplankton.

As shown in figure 6, the spatial distributions become quite different from each other depending on the initial conditions after a long time has elapsed. In this sense, the spatial patterns are very sensitive to the initial distributions. However, it is well known that sensitivity to the initial conditions is an intrinsic property of chaotic systems such as the mathematical model (7)–(9).

4.4 Dependence of spatial pattern on input rate of nutrient

The correlation between the eutrophication level and the spatial phytoplankton distribution in the mathematical model (7)–(9) is examined by changing the input rate of nutrients i_n . Figure 7 shows the simulation results of the spatial patterns for different values of i_n at $t=180$. When $i_n=0.2$, no pattern appears, corresponding to the total extinction of phytoplankton (figure 7a). On the other hand, when $i_n=1.6$, the homogeneous distribution of a large quantity of phytoplankton occurs, reflecting a mass occurrence of phytoplankton blooms (figure 7f). These two extreme cases are directly supported by the results obtained from the mean-field model.

The cases within a limit-cycle oscillation region are more interesting. For example, the cases in $i_n=0.5$ and 0.7 show filamentous patterns (figure 7b, c). In this article, filamentous pattern means a patchiness pattern with locally concentrated and thinly stretched structures. Meanwhile, the case in $i_n=0.9$ seems to be a typical example of a patchiness pattern, in which the stretched and curled structures are widely dispersed (figure 7d). The patchiness pattern becomes obscure gradually with an increase in i_n (figure 7e), reaching a uniformly distributed homogeneous pattern (figure 7f).

Phytoplankton blooms are also controlled by zooplankton predation as well as nutrient input. In this case, the control parameter is the maximum feeding rate of zooplankton on phytoplankton f_p , and a decrease in f_p corresponds to an increase in i_n . Even though the results are not shown, a similar sequence of spatial patterns as that in figure 7 can be recognized. That is, as f_p decreases, the spatial patterns change from no pattern to filamentous patterns, patchiness patterns and homogeneous distributions.

According to Rietkerk *et al* (2004), there is a sequence of vegetation patterns in arid ecosystems that can predict the level of resource availability. Vegetation patterns change

from homogeneous cover to gaps, labyrinths or stripes, and spots, as the resource (such as water or nutrients) input is decreased. Our simulation results show a similar sequence of plankton distribution, such as homogeneous cover, patchiness patterns and filamentous patterns, as the nutrient input is decreased. This observation suggests that the distribution pattern can be an indicator of the eutrophication level in aquatic ecosystems.

5. Conclusions

(i) The present minimal two-component models (5)–(6) and (7)–(9) can simulate the basic features of nutrient–phytoplankton dynamics in aquatic ecosystems and avoid the paradox of enrichment.

(ii) The spatiotemporal simulations show a sequence of spatial patterns as the nutrient input is increased. The spatial distribution of phytoplankton changes from no pattern (extinction of the entire phytoplankton population) to filamentous patterns, patchiness patterns and homogeneous distributions. These observations indicate that the eutrophication level of aquatic ecosystems can be evaluated by the visible patterns of phytoplankton distributions.

(iii) The simpler version of the present model (8)–(9), in which the functional response of nutrient uptake by phytoplankton is replaced by the Holling type I, and the loss term of nutrients is omitted, can create spatiotemporal chaos even without the advection terms. This is a similar example of patchiness-like pattern formation induced only by the diffusion terms, which has already been fully investigated by Medvinsky *et al* (2002) using the Scheffer model.

Acknowledgments

This study is supported by the Global COE Program "Global Eco-Risk Management from Asian View Points" from the Ministry of Education, Culture, Sports, Science and Technology, Japan.

References

- Abraham E R 1998 The generation of plankton patchiness by turbulent stirring; *Nature (London)* **391** 577–580
- Amemiya T, Enomoto T, Rossberg A G, Takamura N and Itoh K 2005 Lake restoration in terms of ecological resilience: a numerical study of biomanipulations under bistable conditions; *Ecol. Soc.* **10** 3
- Bohannan B J M and Lenski R E 1997 Effect of resource enrichment on a chemostat community of bacteria and bacteriophage; *Ecology* **78** 2303–2315
- Bowie G L, Mills W B, Porcella D B, Campbell C L, Pagenkopf J R, Rupp G L, Johnson K M, Chan P W H and Gherini S A 1985 *Rates, constants, and kinetics formulations in surface water quality modeling* 2nd edition (Athens: US Environmental Protection Agency)
- DeAngelis D L, Bartell S M and Brenkert A L 1989 Effects of nutrient recycling and food-chain length on resilience; *Am. Nat.* **134** 778–805
- Dyke P P G and Robertson T 1985 The simulation of offshore turbulent dispersion using seeded eddies; *Appl. Math. Model.* **9** 429–433
- Gentleman W, Leising A, Frost B, Strom S and Murray J 2003 Functional responses for zooplankton feeding on multiple resources: a review of assumptions and biological dynamics; *Deep-Sea Res. II* **50** 2847–2875
- Holling C S 1973 Resilience and stability of ecological systems; *Annu. Rev. Ecol. Syst.* **4** 1–23
- Luckinbill L S 1974 The effects of space and enrichment on a predator–prey system; *Ecology* **55** 1142–1147
- McCauley E and Murdoch W W 1990 Predator–prey dynamics in environments rich and poor in nutrients; *Nature (London)* **343** 455–457
- Martin A P 2003 Phytoplankton patchiness: the role of lateral stirring and mixing; *Prog. Oceanogr.* **57** 125–174
- Medvinsky A B, Petrovskii S V, Tikhonov D A, Tikhonova I A, Ivanitsky G R, Venturino E and Malchow H 2001 Biological factors underlying regularity and chaos in aquatic ecosystems: simple models of complex dynamics; *J. Biosci.* **26** 77–108
- Medvinsky A B, Petrovskii S V, Tikhonova I A, Malchow H and Li B-L 2002 Spatiotemporal complexity of plankton and fish dynamics; *SIAM Rev.* **44** 311–370
- Mullin M M, Stewart E F and Fuglister F J 1975 Ingestion by planktonic grazers as a function of food concentration; *Limnol. Oceanogr.* **20** 259–262
- Neufeld Z, Haynes P H, Garçon V and Sudre J 2002 Ocean fertilization experiments may initiate a large scale phytoplankton bloom; *Geophys. Res. Lett.* **29** 10.1029/2001GL013677
- Okubo A 1971 Oceanic diffusion diagram; *Deep-Sea Res.* **18** 789–802
- Petrovskii S V and Malchow H 1999 A minimal model of pattern formation in a prey–predator system; *Math. Comput. Model.* **29** 49–63
- Petrovskii S V, Li B-L and Malchow H 2004 Transition to spatiotemporal chaos can resolve the paradox of enrichment; *Ecol. Complex.* **1** 37–47
- Rietkerk M, Boerlijst M C, van Langevelde F, HilleRisLambers R, van de Koppel J, Kumar L, Prins H H T and de Roos A M 2002 Self-organization of vegetation in arid ecosystems; *Am. Nat.* **160** 524–530
- Rietkerk M, Dekker S C, de Ruiter P C and van de Koppel J 2004 Self-organized patchiness and catastrophic shifts in ecosystems; *Science* **305** 1926–1929
- Rosenzweig M L 1971 Paradox of enrichment: destabilization of exploitation ecosystem in ecological time; *Science* **171** 385–387
- Roy S and Chattopadhyay J 2007 The stability of ecosystems: a brief overview of the paradox of enrichment; *J. Biosci.* **32** 421–428

- Scheffer M 1991 Fish and nutrients interplay determines algal biomass: a minimal model; *Oikos* **62** 271–282
- Scheffer M 1998 *Ecology of shallow lakes* (Dordrecht: Kluwer Academic Publishers)
- Sigee D C 2005 *Freshwater microbiology* (West Sussex: Jhon Wiley)
- Turing A M 1952 On the chemical basis of morphogenesis; *Philos. Trans. R. Soc. Ser. B* **237** 37–72
- Tzella A and Haynes P H 2007 Small-scale spatial structure in plankton distributions; *Biogeosciences* **4** 173–179
- von Hardenberg J, Meron E, Shachak M and Zarmi Y 2001 Diversity of vegetation patterns and desertification; *Phys. Rev. Lett.* **87** 198101
- Vos M, Kooi B W, DeAngelis D L and Mooij W M 2004 Inducible defences and the paradox of enrichment; *Oikos* **105** 471–480

MS received 3 October 2007; accepted 21 May 2008

ePublication: 28 June 2008

Corresponding editor: JON PAUL RODRÍGUEZ